The Global Atmosphere and Ocean System, 1995, Vol. 3, pp. 55–79
Reprints available directly from the publisher
Photocopying permitted by license only

ROLE OF SEA FLUXES AND TOPOGRAPHY IN EASTERN MEDITERRANEAN CYCLOGENESIS

P. ALPERT, U. STEIN AND M. TSIDULKO
Department of Geophysics and Planetary Sciences
Raymond and Beverly Sackler Faculty of Exact Sciences
Tel Aviv University, Tel Aviv, 69978, Israel.

(Received in final form March 20, 1995)

Four typical Eastern Mediterranean (EM) winter cyclones were simulated, using the NCAR/PSU numerical mesoscale model. They all show a tendency for a sub-synoptic cyclone regeneration over the Mediterranean sea, south of the Cyprus island. This phenomenon is commonly referred to as a 'Cyprus Low', and its origin/mechanisms are investigated.

A sensitivity study was carried out to isolate the effects of topography and surface fluxes on the 'Cyprus Low' development. A recently developed factor separation method was implemented, allowing a quantitative comparison between the contributions of topography and sea surface fluxes along with their synergistic effect to the cyclone's pressure fall. It is shown that the original cyclone, arriving from the west, was mainly influenced by the Turkish mountains whereas the Cyprus development was primarily induced by the Mediterranean sea fluxes. Consequently, a distinct boundary-layer vorticity maximum was found in the 'Cyprus Low', in contrast to the original cyclone which had a mid-tropospheric dominant vorticity centre. Tracks, vorticities, pressure falls and precipitation patterns all indicate the distinct development and mechanisms of eastern Mediterranean cyclogenesis.

KEY WORDS: Cyclogenesis, Mediterranean cyclones, Sea fluxes, Topography, Rainfall

1. INTRODUCTION

Synoptic studies (Petterssen, 1956; U. K. Met. Office, 1962; Reiter, 1975) have shown that the eastern Mediterranean (EM, hereafter) is an active cyclogenetic area during winter. Local meteorologists are familiar with the phenomena of cyclones delayed in the EM en-route eastward. Statistics of winter cyclones in the northern hemisphere show that while the gulf of Genoa is the center with the highest probability for cyclone existence, the EM is the next highest. Figure 1 presents a map with the average number of cyclones for January 00 GMT following a recent study of ECMWF data by Alpert et al. (1990a).

The Mediterranean cyclones may be grouped (Reiter, 1975) according to their origin into (1) those entering from outside the region, especially from the Atlantic; (2) those generated in the western or central Mediterranean, due to local factors like topography and heat fluxes from the large heat reservoir of the Mediterranean sea, often moving further east to the EM; (3) and those developing in the EM region. Most of the EM cyclones were assumed to be of the second type, being generated over the gulf of Genoa. Based on our findings, it is suggested that mesoscale, cyclonic developments in the EM, i.e. of origin (3) are probably most common. It will be shown that the EM development is associated with the enhancement of the local surface moisture fluxes and redistribution of the local precipitation.

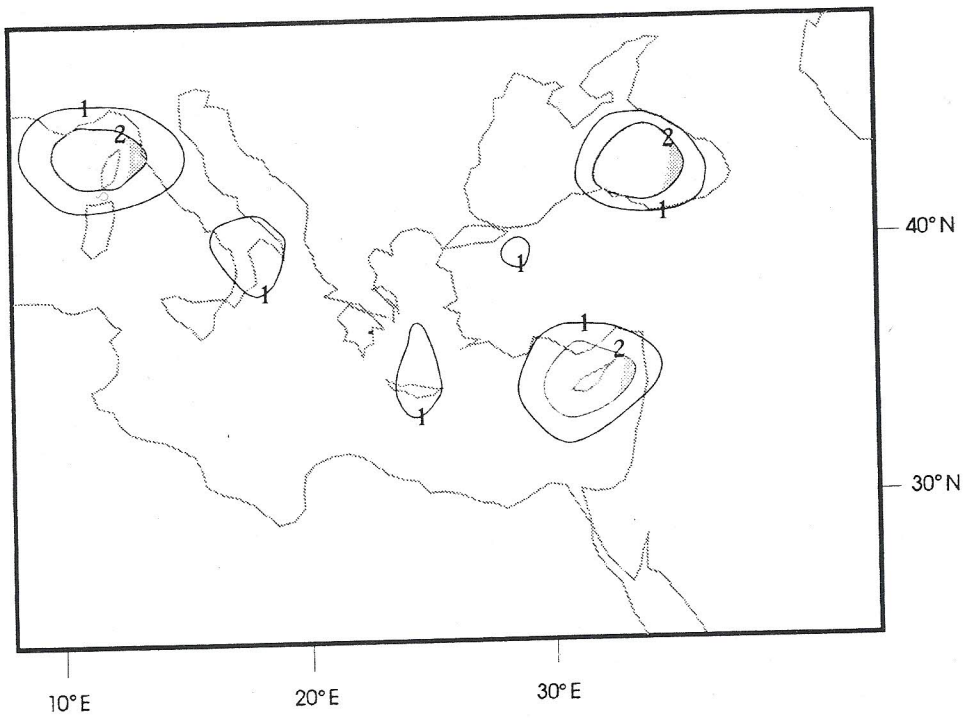

FIGURE 1 Isolines of average number of cyclones for Jan. 00 UTC following Alpert et al. (1990a). Regions where number is greater than 2, are shaded. Number of cyclones is for a unit area of 250 × 250 km.

Our purpose here is to investigate the role played by the topography and the sea fluxes in EM cyclogenesis. A brief description of the two primary mechanisms, i.e. topography and sea fluxes, follows. A more detailed review can be found in Radinovic (1987) and Alpert and Warner (1986).

Cyclone statistics over the region show high correlation with topography (Godev, 1970). The pressure in the lee of the mountains tends to fall thus leading to cyclone development. A few theories have been proposed to explain this so called lee cyclogenesis phenomena (e.g., Smith, 1984; Tafferner and Egger, 1990) and a number of numerical studies have been performed with satisfactory simulations. A central problem in these studies is the appropriate isolation of topographic effects from other factors (Stein and Alpert, 1993, henceforth SA and Alpert et al., 1995) and the quantitative estimation of their relative importance. Some studies (Buzzi and Tibaldi, 1978; Tibaldi et al., 1990) attribute the lee cyclogenesis, at least in its first phase, to the blocking of the cold front by the mountain ridge. This explanation does not seem to apply, in general, to the EM because the cold front when entering the region from the west is not blocked by the Turkish mountains, (Figure 2). Several studies simulate Alpine lee cyclogenesis (Egger, 1972; Radinovic, 1965; Tibaldi et al., 1980, Tibaldi et al., 1990). However, they cannot be directly applied to the EM cyclogenesis because of the major differences between the regions. In the present study the role of the Turkish Mountains in the EM cyclogenesis is investigated.

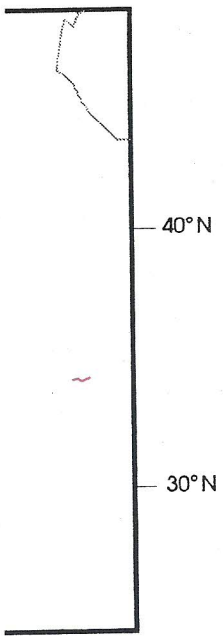

rt et al. (1990a). Regions of 250 × 250 km.

graphy and the sea ry mechanisms, i.e. found in Radinovic

opography (Godev, leading to cyclone called lee cyclogen- and a number of ons. A central prob- effects from other al., 1995) and the (Buzzi and Tibaldi, ts first phase, to the n does not seem to the region from the al studies simulate , 1980, Tibaldi et al., nesis because of the role of the Turkish

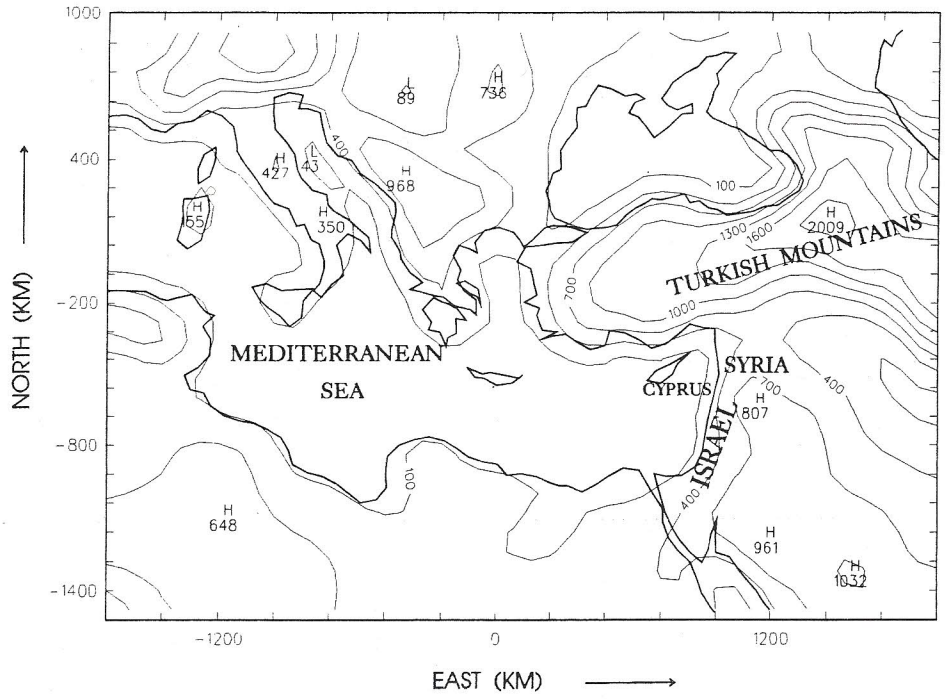

FIGURE 2 Model domain and topography with a contour interval of 300 m. Horizontal east-west and south-north scales are in kms relative to the grid's center. Latitudes and longitudes are given in Figure 4.

The possible cyclogenetic role of the Mediterranean heat reservoir in the EM is reviewed next. The average SST in the EM in October is 25°C (Reiter, 1975). This temperature is about 20°C higher on the average than the land surface temperature to the north of the region (i.e. the Turkish mountains) and about 5°C warmer than the western Mediterranean. An example of the land surface temperature for the 5 Jan 1987 simulation is given in Section 5, Figure 13. The SST data are from the U. S., Navy for early Jan 1987. Such a large difference between land and sea temperature favors polar-type cyclonic development (Alpert and Neeman, 1992). Rassmussen (1979), referring to polar lows, argues that airmasses crossing the ice-line to the warmer sea induce thermal instability triggering cyclone development in which CISK (Conditional Instability of the Second Kind) plays the major role. This can, in some cases, also apply to the EM, as suggested by Alpert (1984), particularly with a northerly prevailing flow. A somewhat similar approach to EM cyclone generation was proposed by Levich and Tzvetkov (1985). They suggested that the interaction between the sea and the cold air flowing from the north, first induces the cloud generation. The cumulus clouds, with a horizontal scale of 1–3 km, extract energy stored in the Mediterranean heat reservoir primarily through the latent heat fluxes. In turn, this energy cascades from the small meso-γ cloud scale to larger scales and generates meso-β cyclones of the order of 100–200 km. This idea, however, has not yet been substantiated.

In the present paper sensitivity studies for four EM cyclonic cases are performed applying the factor separation method. By allowing the separation of the synergistic

contributions the method provides, for the first time, a quantitative comparison of several factors, see SA. The factors under test were consequently chosen to be the topography and the surface heat fluxes. Cyclogenesis was diagnosed by following the simulated sea level pressure change, relative vorticity and accumulated rainfall. The contribution of each factor to the pressure change at the cyclone center was calculated.

A typical EM cyclogenetic case is presented (Section 2), then simulated by the mesoscale NCAR/PSU model (Section 3). Through the factor separation method (Section 4) the pressure at the cyclone center is described as the sum of four contributions due to topography, fluxes, fluxes/topography interaction, and the contribution independent of the two factors. This last contribution will be referred to briefly as the large-scale contribution, since the dominant local factors were excluded. Finally, the fields of relative vorticity and rainfall were explored (Section 5). Section 6 summarizes the main results.

2. SURFACE OBSERVATIONS OF EM CYCLOGENESIS

During an average winter about 10 synoptic-scale cyclones pass through the EM, most of type (2), i.e. generated over the WM. Four cyclonic cases were arbitrarily chosen and could be considered as typical cyclones in the EM, generally named by local forecasters "Cyprus lows" (Alpert et al., 1990a,b). Each "Cyprus low" contributes on the average 10% of the annual precipitation in the region, i.e. about ~ 50mm at the central coast of Israel. The surface cyclones are, in general, associated with upper level deep troughs from Europe towards the EM. Selected cyclones were chosen from over 60 diagnosed by Shay-El and Alpert (1991). All of the cyclones meet three criteria: a near-Cyprus path, substantial rainfall in Israel (more then 30 mm), and an EM duration of 24 to 48 hours. Although Israel is at the southern edge of most storms, its northern part is generally within the main precipitation area of these storms.

One of the "Cyprus low" cases to be simulated is on the 5 Jan 1987 (Figure 3). In Figure 3a the cyclone was located east of the island of Crete with a central surface pressure of 1008.5 hPa. Twelve hours later (Figure 3b) the cyclone moved quickly northeast along the Turkish coast, deepening to 1007.3 hPa. Next, (Figure 3c), the following occurred; the cyclone left its original track, moved about 300 km to the south and deepened by 5 hPa within 12 hours. This change was significant since otherwise the cyclone would have already left the EM region and its local influence would be quite limited, see Stein and Alpert (1991). The cyclone's delay in the region, its movement southward to Cyprus and the deepening, are typical manifestations of EM cyclogenesis. An important question arises; Is the deepening to the south due to a new (secondary) cyclone generation or is it the original cyclone? To address this question numerical simulations with high temporal resolution and with increasing spatial resolutions are employed (Section 3). In the additional three cases similar delays and/or deepenings were noticed over the Cyprus region. The ECMWF (European Centre for Medium-Range Weather Forecasts) maps were checked against surface weather maps and found to represent the *synoptic* developments quite well.

ntitative comparison of
uently chosen to be the
diagnosed by following
ıd accumulated rainfall.
the cyclone center was

ı, then simulated by the
ıctor separation method
the sum of four contribu-
ion, and the contribution
e referred to briefly as the
ere excluded. Finally, the
ı 5). Section 6 summarizes

ESIS

pass through the EM, most
were arbitrarily chosen and
/ named by local forecasters
contributes on the average
50mm at the central coast of
th upper level deep troughs
sen from over 60 diagnosed
hree criteria: a near-Cyprus
an EM duration of 24 to 48
storms, its northern part is
ms.
he 5 Jan 1987 (Figure 3). In
Crete with a central surface
the cyclone moved quickly
ı hPa. Next, (Figure 3c), the
ed about 300 km to the south
significant since otherwise the
ocal influence would be quite
y in the region, its movement
ınifestations of EM cyclogen-
to the south due to a new
one? To address this question
ı and with increasing spatial
ıree cases similar delays and/or
CMWF (European Centre for
l against surface weather maps
e well.

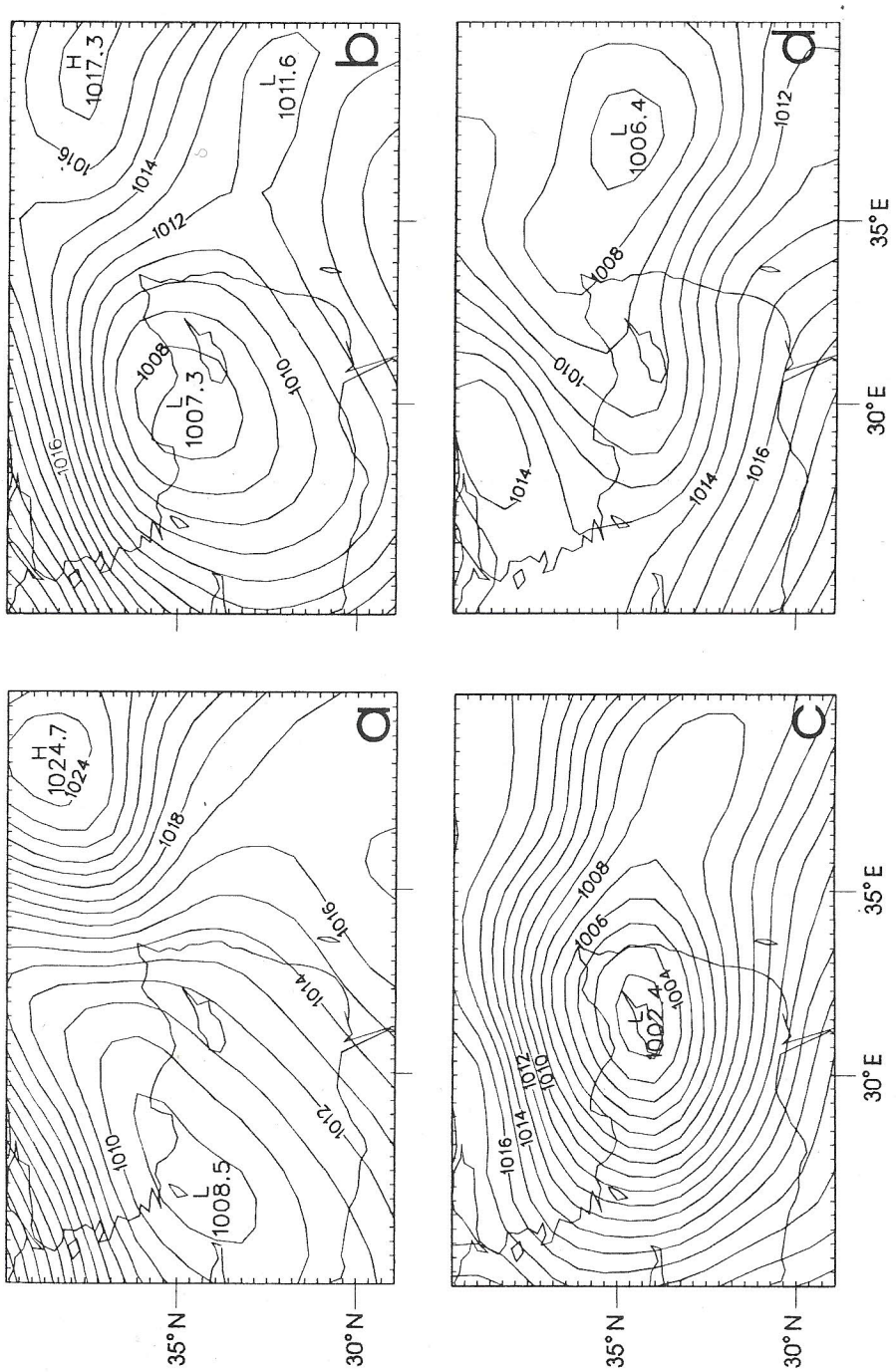

FIGURES 3a,b,c,d Sea level pressure charts for case (a) based on ECMWF analyses with 12 h interval, starting at 00 UTC: (a) 5 Jan 1987 00 UTC; (b) 5 Jan 1987 12 UTC; (c) 6 Jan 1987 00 UTC; (d) 6 Jan 1987 12 UTC. Contour interval is 1 hPa.

3. MODEL SIMULATIONS

a. Some numerical and modelling aspects

For the initialization and lateral boundary conditions, the ECMWF initialized analyses with a 2.5° grid interval were employed by interpolating the data to the mesoscale grid intervals of 80, 40 and 20 km. Numerical simulations of 36 h integration time were made using the Pennsylvania State University/National Center of Atmospheric Research (PSU/NCAR) mesoscale model version 4 (MM4), Anthes et al. (1987). The model was run on the EM domain $0° - 55°$ E and $20° - 55°$ N with a mesh of $31 \times 45 \times 16$ grid points with 80 km interval. The same number of grid points were in the 40 km interval while for the 20 km interval a 51×76 horizontal grid was chosen. In all simulations the model domain centre was the same, i.e. (37.3° N, 32.4° E). With a 120s time step ~ 2 CPU hours on an IBM RS/6000 workstation were required for a 36 h run with the 80 km interval. The model domain and topography are shown in Figure 2. Figure 4 illustrates the significant topographical variations with increasing the horizontal resolution. For instance, peaks of 1621, 1804 m are found along the Turkish coast with the 20 km resolution (Figure 4c) compared to only about half the altitude with the 80 km interval. Topography is based on the US Navy 5' resolution following the MM4 option for Cressman interpolation. The four cases simulated and discussed are: (a) 5 Jan 1987 00 UTC–6 Jan 1987 12 UTC; (b) 17 Jan 1983 00 UTC–18 Jan 1983 12 UTC; (c) 17 Jan 1984 00 UTC–18 Jan 1984 12 UTC; (d) 25 Jan 1987 00 UTC–26 Jan 1987 12 UTC. In all cases both 80 and 40 km horizontal intervals were employed. In case (a) a 20-km run was also performed. During the 36 h simulation time the cyclones passed the EM from west to east/northeast.

The version of the model used in this study utilized the modified Kuo (1974) cumulus parameterization (Anthes, 1977), the high resolution boundary layer model, 15 vertical layers and relaxation lateral boundary conditions. The first kilometer above the surface occupies about five layers with the lowest at the mid-level of ~ 40 m. The five lowest layers are located between the sigma levels 1.0, 0.99, 0.98, 0.96, 0.93 and 0.89. The boundary layer parameterization follows Zhang and Anthes (1982) including different treatments for stable and unstable conditions.

The PSU/NCAR mesoscale model simulations will now be discussed, with the aid of the sea level pressure charts.

b. 5 Jan 1987 simulation

The 5 Jan 1987 cyclone moved along the southern coast of Turkey generating a trough toward Cyprus. Figure 5a differs from the analyzed map over the high mountains at the northeast (Figure 3a) due to the model output interpolation from pressure coordinates to sigma and back. At 18 UTC, Figure 5b, the cyclone was located about 100 km north of the southern coast of Turkey. A secondary deepening appeared south of Cyprus (Figure 5b) with its trough to the east. Later, the cyclone remained double centered, and while the primary (northern) center was nearly stationary, the secondary center moved to the northeast (Figure 5c-e). It should be noted that the secondary cyclone deepened by only about 1.5 hPa through the simulation. The observed cyclone's deepening of 6.1

/F initialized ana-
:a to the mesoscale
egration time were
Atmospheric Re-
. et al. (1987). The
J with a mesh of
grid points were in
grid was chosen. In
° N, 32.4° E). With
were required for a
aphy are shown in
ons with increasing
re found along the
only about half the
Navy 5' resolution
:ases simulated and
in 1983 00 UTC–18
; (d) 25 Jan 1987 00
ontal intervals were
36 h simulation time

Kuo (1974) cumulus
er model, 15 vertical
ter above the surface
0 m. The five lowest
0.93 and 0.89. The
2) including different

ussed, with the aid of

y generating a trough
ligh mountains at the
pressure coordinates
l about 100 km north
ired south of Cyprus
. double centered, and
ondary center moved
ary cyclone deepened
one's deepening of 6.1

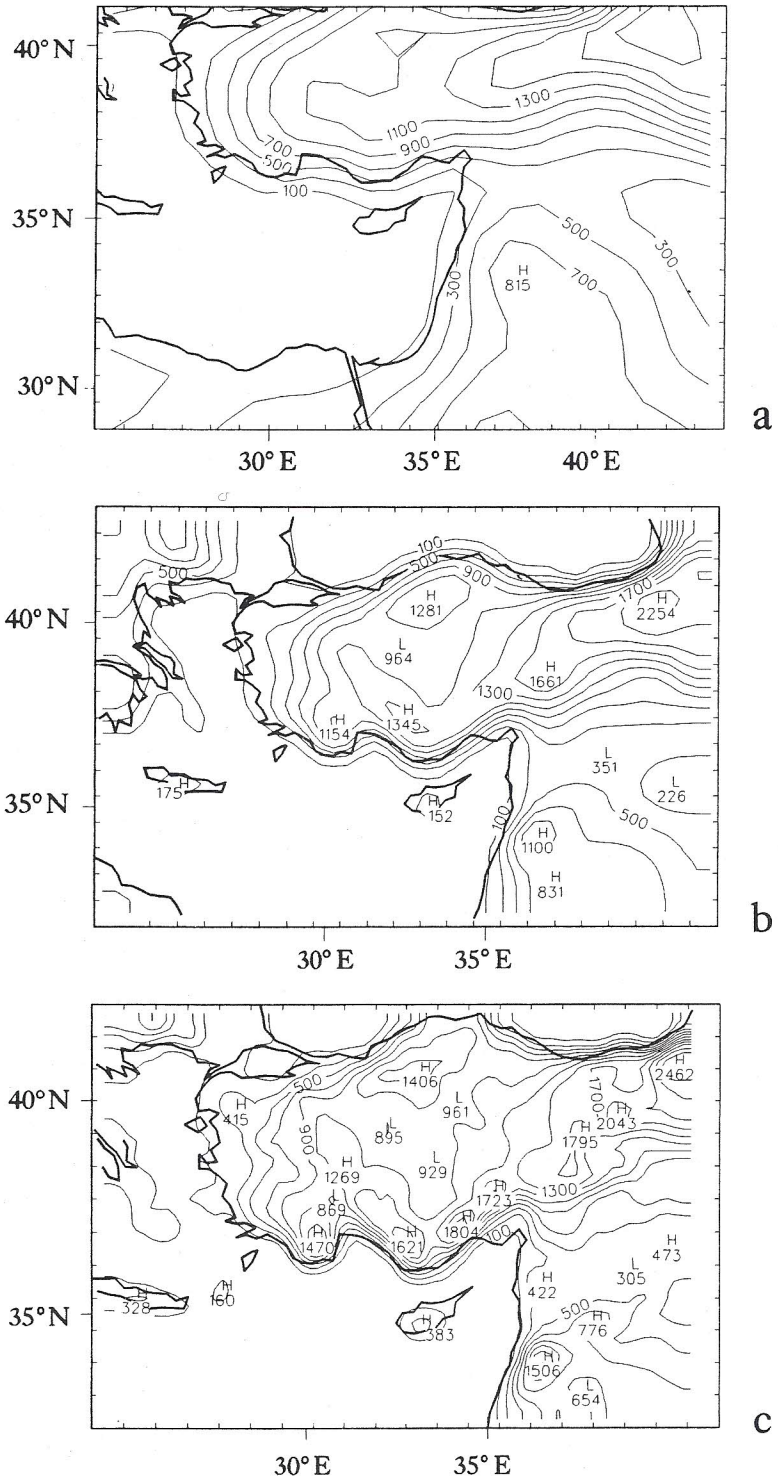

FIGURE 4 As in Figure 2 but with various horizontal resolutions. The horizontal intervals are (a) 80 km; (b) 40 km and (c) 20 km. Contour interval is 200 m.

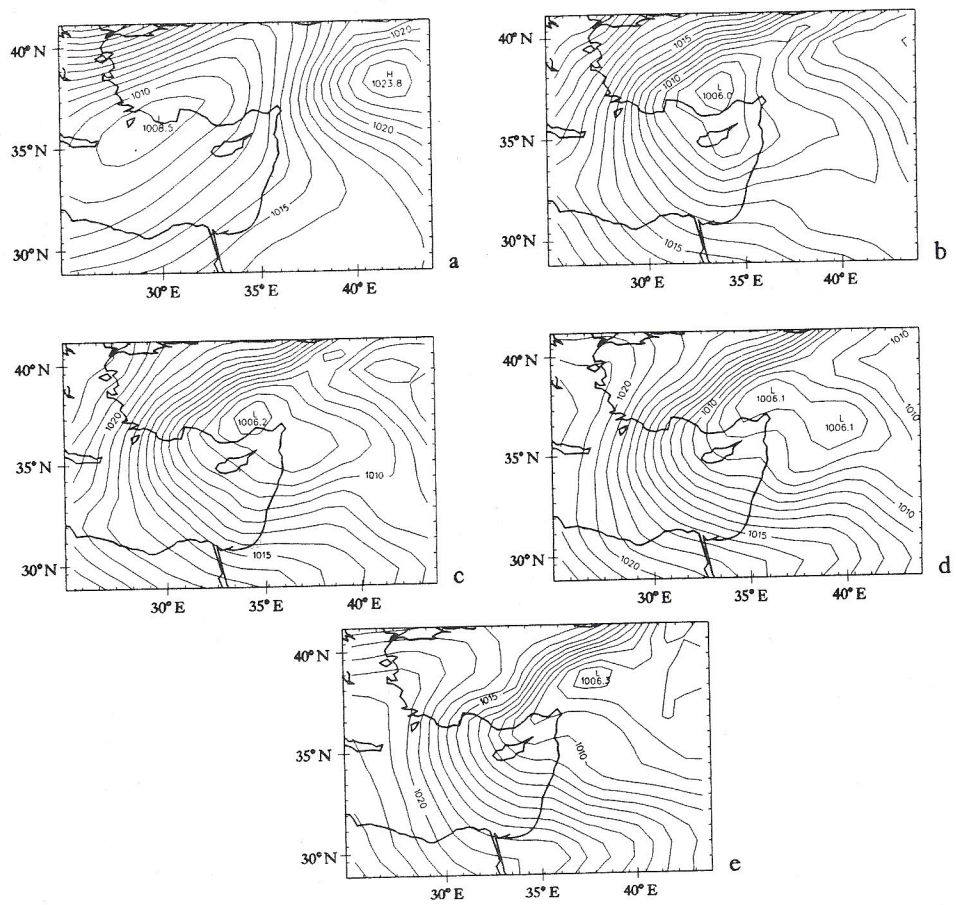

FIGURES 5a,b,c Sea level pressure maps simulated for the first case -5 Jan 1987 00 UTC as follows: (a) Initial map; (b) 18 h simulation; (c) 24 h simulation; (d) 30 h simulation and (e) 36 h simulation. Contour interval is 1 hPa.

hPa was not predicted well in the simulation (Figure 3c). Figures 5c,e can be verified by comparison to Figures 3c,d respectively.

A doubling of the horizontal resolution to 40 km interval and even further to 20 km have not yielded the observed deepening. The 18 h simulated surface pressure charts with the 80, 40 and 20 km grid intervals are shown in Figure 6a, b, c respectively. Although the higher resolutions failed to simulate the Cyprus low deepening (to ~ 1005 hPa), they certainly present a more pronounced secondary development there. In contrast to the 80 km simulation, where the primary cyclone is still dominant at 1006 hPa (Figure 6a), the higher resolutions (Figures 6b,c) suggest that the Cyprus secondary deepening dominates. This corresponds well to the observations in Figure 3c where the ECMWF 24 h analyzed map shows the 1002.4 hPa centre over Cyprus. The three resolutions i.e. 80, 40 and 20 kms yielded 1006.2, 1006.9 and 1006.6 hPa respectively for

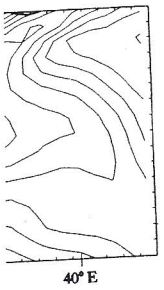

b

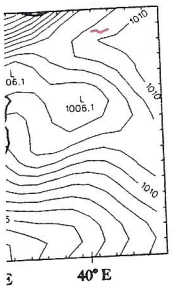

d

00 UTC as follows: (a)
h simulation. Contour

e can be verified by

en further to 20 km
face pressure charts
a, b, c respectively.
leepening (to ~ 1005
velopment there. In
ill dominant at 1006
ne Cyprus secondary
Figure 3c where the
r Cyprus. The three
hPa respectively for

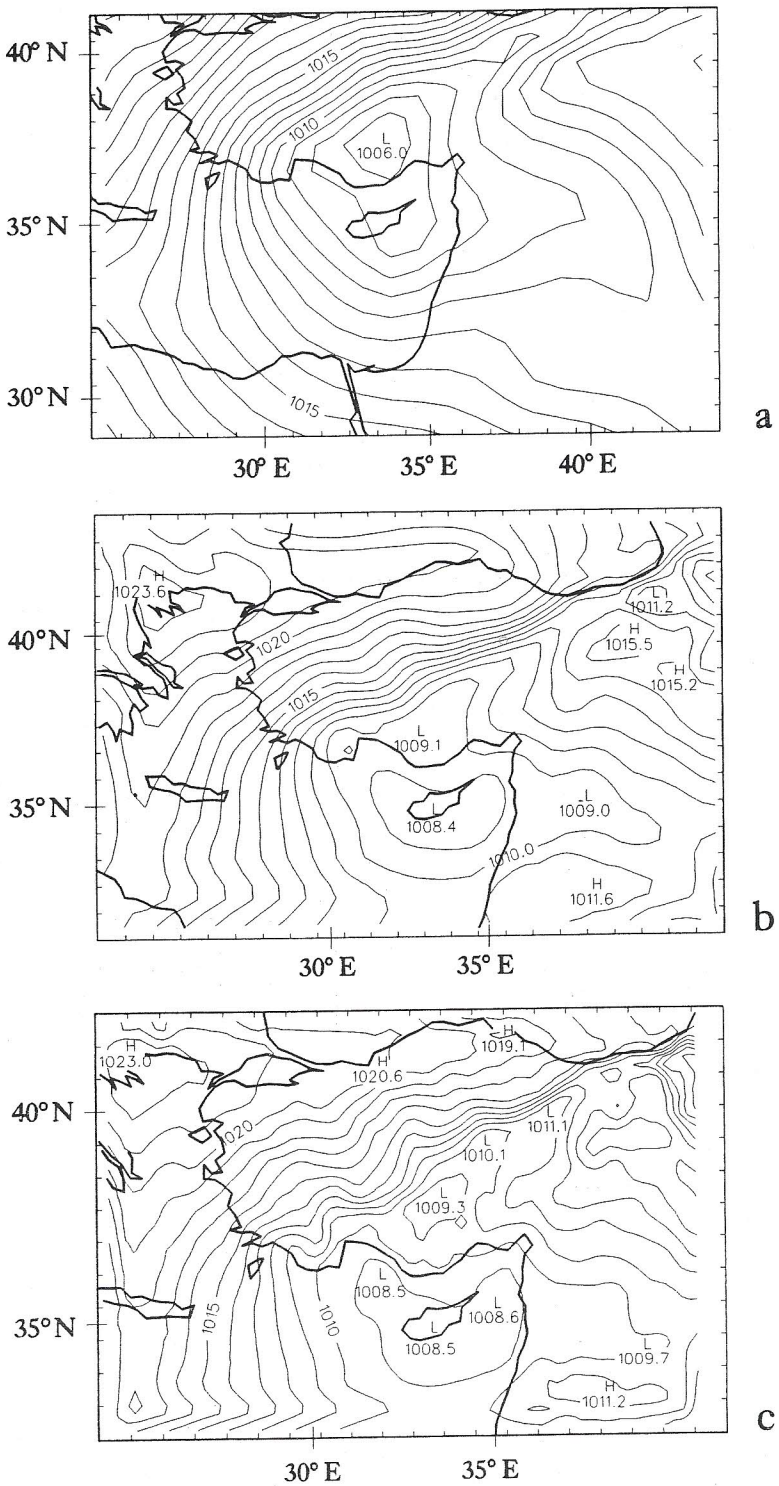

FIGURE 6 As in Figure 5 but for various horizontal resolutions and at the inception time of the secondary Cyprus system, i.e. 18 h. Horizontal intervals are (a) 80 km; (b) 40 km; (c) 20 km.

the + 24 h cyclone's centre (not shown) but the major contrast in location remained. That means, the 80 km center was over Turkey, not Cyprus as observed and simulated by the 40 and 20 km simulations. It should be emphasized however, that since the pressure depth over Turkey depends heavily on the extrapolation to sea level, a potential extrapolation bias affects this result.

c. *Additional cases*

The other three cases of typical EM winter cyclones, were simulated. All share a few common properties, the most evident being the generation of a secondary minimum in the same region. Notice that only in the 5 Jan 1987 case (Figure 7a) the track of the secondary cyclone was somewhat artificially extrapolated in time, even to 12 h earlier than its inception near Cyprus-compare to Figures 5a,b. Another feature relates to the path of the main cyclone; in all cases it moved along the lee side of the Turkish mountains, independent of its initial location, Figure 7. The simulations do predict the appearance of the cyclone in the Cyprus region, but they often underestimate its central pressure. Observational evidence for this deepening, apart from the Cyprus observations and one or two ship reports is lacking. The available reports for wind and pressure do, however, support the existence of a secondary meso-scale minimum. It should be emphasized, regarding the problem of the model verification, that the simulations presented here are with grid intervals of 80, 40 and 20 km, while surface measurements are scarce over sea and the available ECMWF data is with 2.5° interval. The mesoscale model should therefore be considered as a primary research tool for studying such meso cyclogenesis as suggested by Keyser and Uccellini (1987). The model has been operational twice daily in Israel for more than 2 years but its verification is beyond the scope for this study.

4. FACTOR SEPARATION FOR TERRAIN AND SURFACE FLUXES

To analyze the influence of local factors on the aforementioned events, the factor separation method was applied. It utilizes numerical simulations to obtain the individual contribution of any factor to any predicted field, as well as the contributions due to the mutual interactions among two or more factors. In SA the method was developed, and it was shown that 2^n simulations are required in order to separate and calculate the contributions of n factors and their possible interactions.

The factors chosen for the present sensitivity studies are naturally the surface heat fluxes (latent & sensible) and topography. The predicted field in this section is the surface pressure change from the initial time. The primary cyclone and secondary minima were then separately analyzed. For each of them, the central pressure change was predicted employing the four (2^2) simulations required: control; surface fluxes switched off; topography leveled; and the simulation where both fluxes and topography were switched off. In the no-flux simulations, the surface fluxes were set to zero everywhere in the model and no prior time for equilibrium, was allowed. The reason for that is that all the factor-separating simulations are required to start at the same time and with the same initial conditions (see SA).

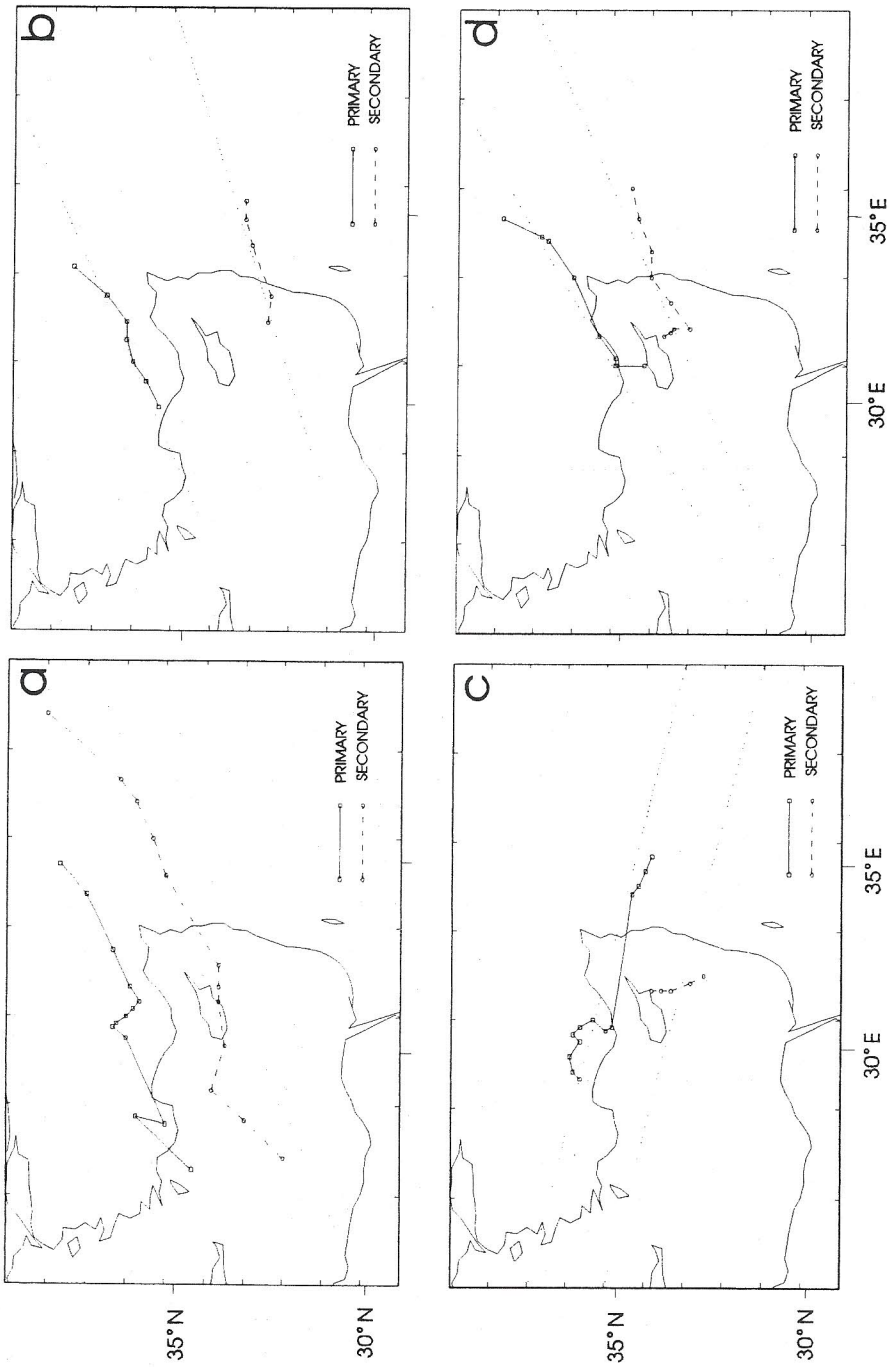

FIGURES 7a,b,c,d Trajectories of the main and secondary systems for (a) 5 Jan 1987; (b) 17 Jan 1983; (c) 17 Jan 1984; (d) 25 Jan 1984. Dotted lines crossing the trajectories represent cross section lines for Figures 8,9. Positions are indicated every 3 h with a dot. All runs are with 80 km interval.

Diagrams for the contributions to pressure change with time for the primary cyclone centre for each case are shown in Figures 8a, b, c, d. Each graph shows the control (bars) as well as the factor-separated results: fluxes effect (stars) topography effect (squares) and the fluxes/topography interaction (triangles). It should be emphasized that each bar represents the pressure change at the cyclone's centre at the pertinent time relative to the initial value *at this point*; not the lagrangian change as is often used. The effect due to other factors ('large scale') is not plotted since we focus on local factors. Similar plots for the secondary minima are given in Figures 9a, b, c, d. In each of the diagrams the value of the pressure fall in the control run is equal to the sum of the four contributions: fluxes, terrain and their interaction along with the fourth 'large scale' contribution. The latter can be obtained from subtracting the sum of the 3 local contributions from the control result.

In case (a), Figure 8a, the pressure drop at the cyclone centre (as defined earlier) continues throughout the simulation, while stronger drops occurred between 6–18 and 24–33 h. Figure 8a shows that the fluxes and the interaction contributions were negligible, while that of the topography was dominant. During the first 27 hours the pressure fall is mainly due to topography, followed by the contribution due to the 'large scale'. In case (b), Figure 8b, the pressure fall due to the fluxes is also negligible but the topography contributed negatively to the pressure fall, i.e., raising the pressure. The main contributor here, is the interaction. In case (c), as in (a), the pressure fall is prominent during the periods 0–15 and 24–27 h. The first drop is due to both topography and interaction, while the fluxes contribution is negligible. The second drop however, is due to the fluxes, in contrast to the other local factors which contributed negatively. In case (d), the fluxes contribution to pressure change was also small and the main factor is again the topography.

Figure 9a presents similar diagrams but for the secondary minimum. In case (a) a significant pressure fall of 5 hPa, is found at 3–18 h. The main contributor to this pressure fall is fluxes, while other factors are secondary. In case (b), in both periods of pressure fall, the fluxes factor dominates. In case (c), Figure 9c, the period of pressure fall is 0–15 h, and again, prior to 12 h the fluxes is the main contributor while from 15 h on, the interaction dominates. The fluxes are the main factor prior to 12 h in case (d), as well. Later on, topography becomes dominant.

In summary, diagrams 8–9 show that the dominant factor varies throughout the simulation. The various contributions are compared at critical times of development. For the primary cyclone this was time of maximum deepening (largest negative bar), and for the secondary minimum its time of appearance. In this way, the factors contributing to the primary cyclone's *deepening* and those contributing to the secondary *generation*, are illustrated. The contributions of the factors were ordered (Tables 1, 2) so that the largest contributor to deepening is denoted as no. 1. The main contributors for the primary cyclone deepening (Table 1) are terrain and terrain-fluxes interaction, while the fluxes contribution is weakest. In the secondary generation, however, the order is quite different and in all cases the fluxes were dominant. Other components appear in exactly the same order for all cases, i.e. the second component is the terrain-fluxes interaction while terrain is last. If, however, the maximum deepening phase was chosen here as well then the terrain contribution still remained no. 3 for the secondary development, except for the fourth event.

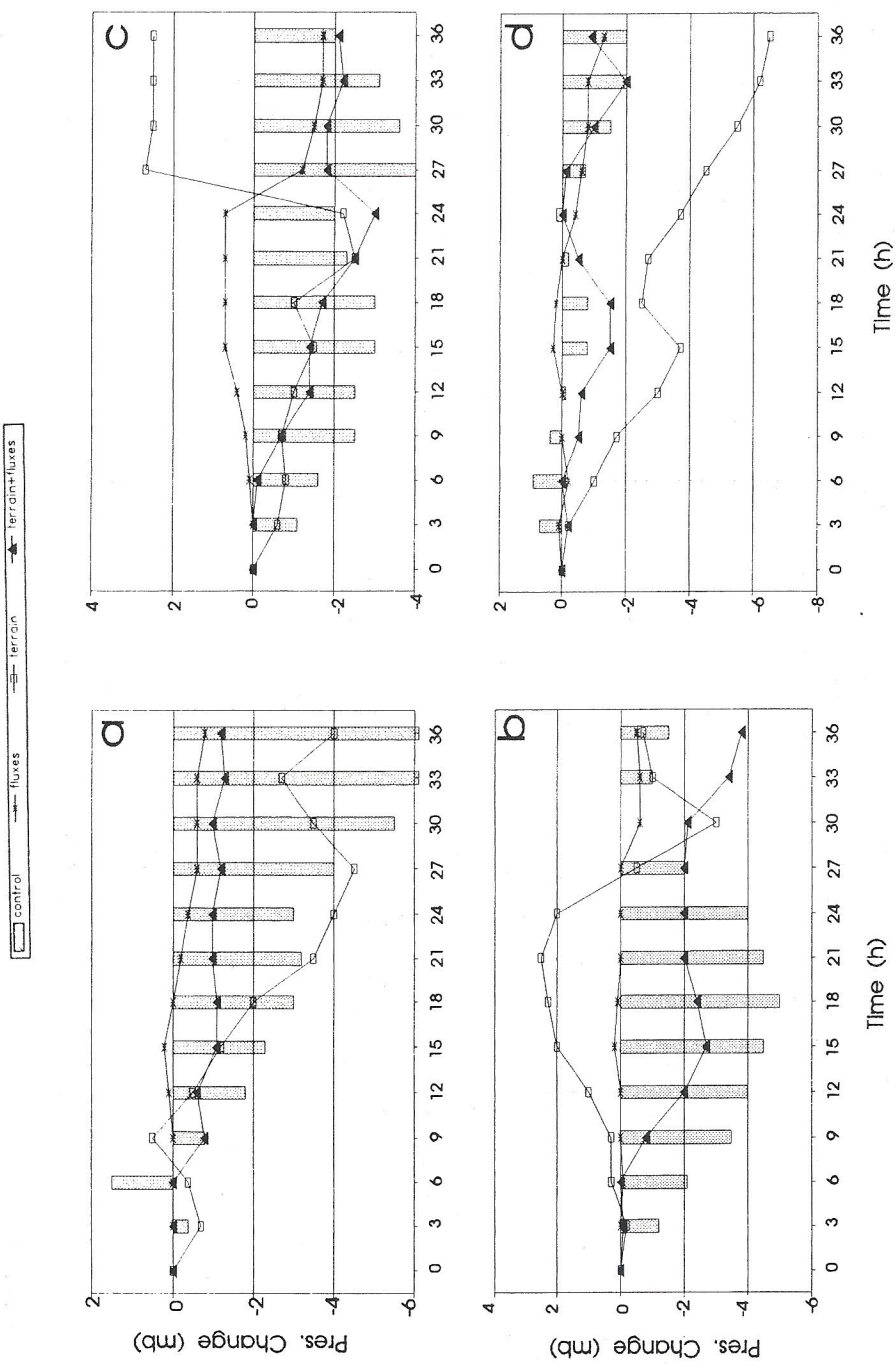

FIGURES 8a,b,c,d Diagrams of pressure change at the cyclone's centre for each of the four cases in hPa (mb) units. The pressure change in the control run (bar), due to fluxes (stars) due to terrain (squares) and due to the terrain/fluxes interaction (triangles) are plotted for the four cases: a) 5 Jan 1987; b) 17 Jan 1983; c) 17 Jan 1984; d) 25 Jan 1984. Runs are with 80 km interval.

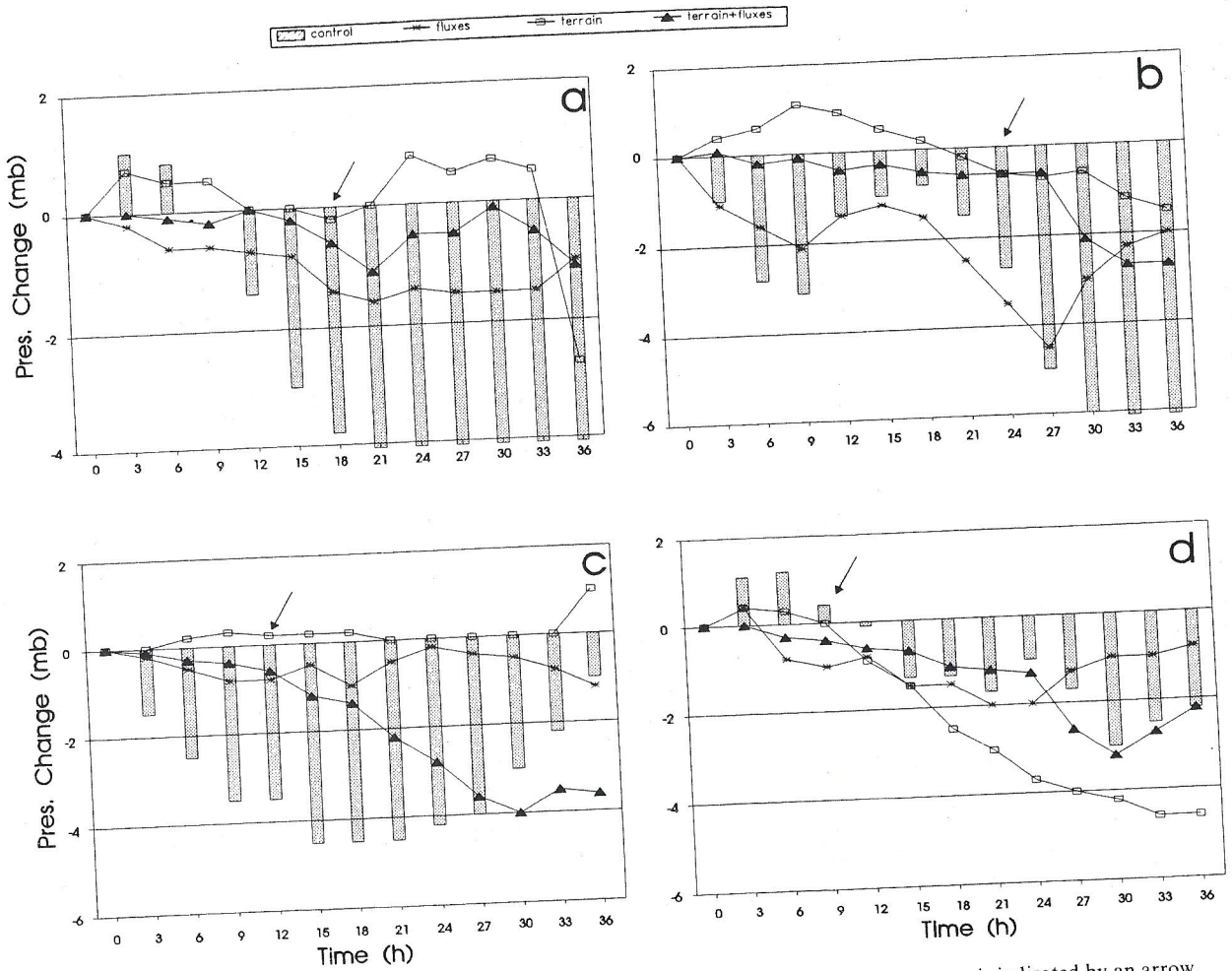

FIGURES 9a,b,c,d As in Figure 8 but for the secondary system. Time of cyclone's first appearance is indicated by an arrow.

TABLE 1

The sequel of factors for each case contributing to the pressure change at the centre of the primary cyclone at time of maximum deepening, following Figure 8.

Case	Prediction time	No. 1	No. 2	No. 3
5 Jan 87	36	terrain	terrain-fluxes	fluxes
17 Jan 83	18	terrain-fluxes	fluxes	terrain
17 Jan 84	27	terrain-fluxes	fluxes	terrain
25 Jan 87	33	terrain	terrain-fluxes	fluxes

TABLE 2

As in Table 1 except for the secondary development at time when minimum first appeared, following Figure 9.

Case	Prediction time	No. 1	No. 2	No. 3
5 Jan 87	18	fluxes	terrain-fluxes	terrain
17 Jan 83	24	fluxes	terrain-fluxes	terrain
17 Jan 84	12	fluxes	terrain-fluxes	terrain
25 Jan 87	9	fluxes	terrain-fluxes	terrain

To further illustrate this major difference between the primary and the secondary cyclones the vorticity vertical cross-sections are examined next. The large-scale and topographically forced vorticity distributions are expected to be quite different from that of a circulation generated mainly by the sea fluxes.

5. VORTICITY CROSS-SECTIONS AND RAINFALL DISTRIBUTIONS

The primary and secondary cyclone trajectories for the 4 cases are shown in Figure 7. Both tend to stay in their more favourable area, i.e. the primary cyclone along the southern slopes of the Turkish mountains while the secondary minimum follows an over water route to the south of Cyprus. The trajectories are in agreement with earlier diagnoses (Alpert, 1989; Alpert et al., 1990b). The relative vorticity cross sections were plotted along the dotted lines from Figure 7, the northern for the primary cyclone (Figure 11) and the southern, for the secondary one (Figure 10). Cross-sections were chosen for the 24 h simulation time when cyclones were quite developed, except for case (c) at 12 h because later on, the cyclone has significantly changed its path, Figure 7.

Figures 10a, b, c, d present vertical cross sections along the trajectories of the secondary minimum. Areas of high vorticity (larger than 6 in vorticity units of $10^{-5}s^{-1}$), are shaded. In case (a), Figure 10a, the region of strongest vorticity is located near 300 hPa, with a maximum value of 11.4. This region of high vorticity is related to the main cyclonic system. One region of high vorticity is east of Cyprus, beneath the 800 hPa level, and the other is to the west. The maximum vorticity at low levels (6.9 units), is smaller than the high level vorticity maximum. In case (b), Figure 10b, the main vorticity maximum of 9.3 is again at high levels, around 400 hPa. Here also there is

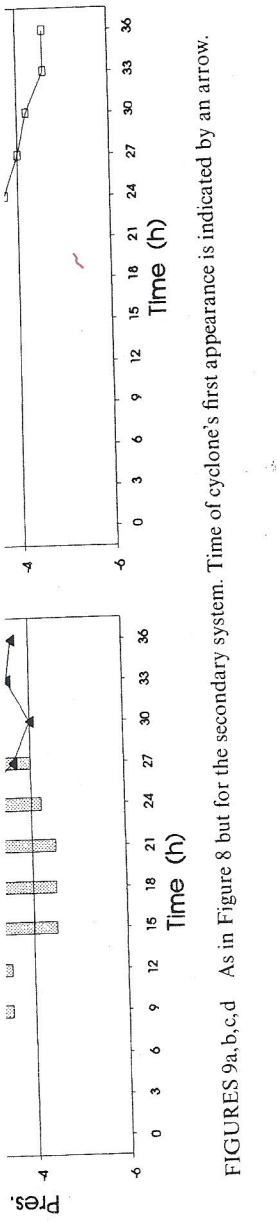

FIGURES 9a,b,c,d As in Figure 8 but for the secondary system. Time of cyclone's first appearance is indicated by an arrow.

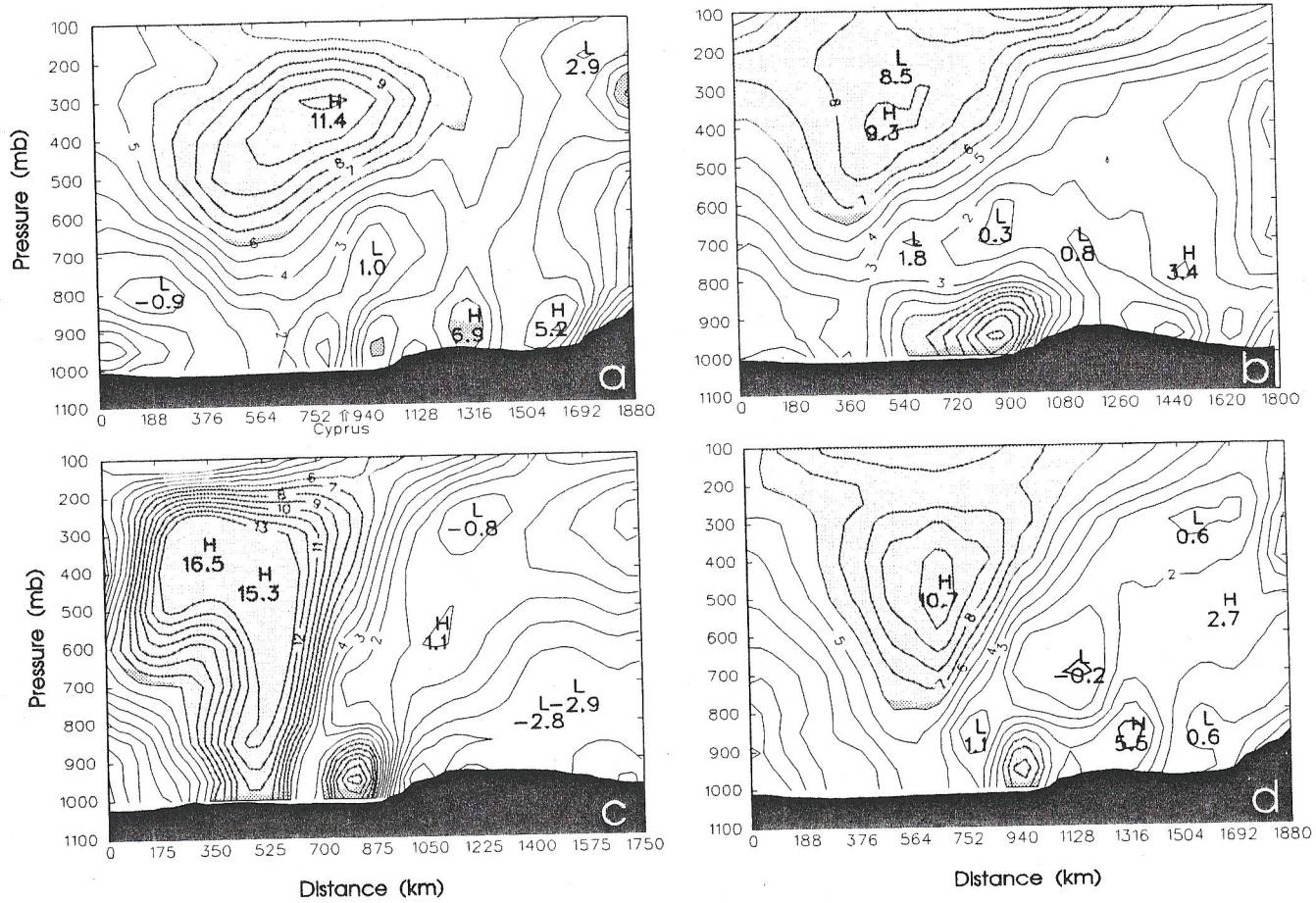

FIGURES 10a,b,c,d Cross sections of relative vorticity for the secondary systems along cross-section lines given in Figure 7 for (a) 5 Jan 1987 + 24h; (b) 17 Jan 1983 + 24h; (c) 17 Jan 1984 + 12h; (d) 25 Jan 1984 + 24h. Shaded area denotes relative vorticity exceeding 6 ($*10^{-5}s^{-1}$) units. Runs are with 80 km interval.

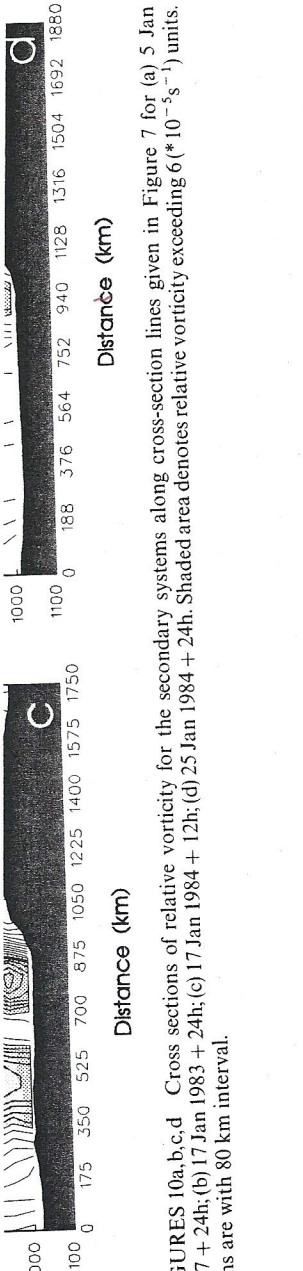

FIGURES 10a,b,c,d Cross sections of relative vorticity for the secondary systems along cross-section lines given in Figure 7 for (a) 5 Jan 1987 + 24h; (b) 17 Jan 1983 + 24h; (c) 17 Jan 1984 + 12h; (d) 25 Jan 1984 + 24h. Shaded area denotes relative vorticity exceeding 6 (* $10^{-5}s^{-1}$) units. Runs are with 80 km interval.

a region of high vorticity at low levels that is located east to the higher maximum. The position of the low level maximum is above Cyprus, reaching 12, a value even higher than that for the high level maximum. In case (c), Figure 10c, the high vorticity region extends down to low levels and, as in the other cases, another vorticity maximum is found east of the high level maximum and near Cyprus. A similar picture was found in the fourth case as well, Figure 10d.

Comparing Figures 10 and 11 shows consistent differences between the two systems. The primary cyclone is mainly influenced by the upper level large scale synoptic system. The region of high vorticity is connected to the main convective centre at the cold front, and extends through the whole troposphere, as is typical of mid-latitude cyclones in general. Cross sections of the secondary minima, however, show two centres, one related to the upper level trough of the main synoptic system, and the other to the low-level system developing over the Cyprus region. The separation between the systems suggests that the latter may have been induced by local processes. This low level vorticity centre is probably associated with the boundary layer processes and this is supported by Table 2, which shows that the dominant factor for the secondary development is the surface fluxes. In two of the cases (b and c) the intensity of the low level vorticity centre have even reached the value of 12 which is larger than the corresponding upper-level centre. This can potentially result from feedback processes operating between the secondary development and the fluxes in the following manner: the centre intensifies the fluxes by convective processes and the wind strengthening. Larger sea fluxes destabilize the lower troposphere through boundary layer heating, and lead to a pressure fall following latent heat release by the convective processes.

Further understanding of the secondary minima over Cyprus can be obtained from comparing the SST and sea fluxes at time of inception with the idealized favourable patterns examined by Nuss (1989). He investigates three cases of idealized marine cyclones with two patterns of SST and surface heat fluxes. One pattern uses a zonal SST distribution, upward fluxes to the west of the surface low and downward fluxes to the east of the surface low; another is a sinusoidal SST distribution, large upward heat fluxes to the north as well as west of the surface low. Nuss's experiments show that the first pattern of heating acts to oppose the cyclogenesis. The cyclone moves toward colder water, it increases downward flux to the east of the low and decreases upward flux to the west of the low. This pattern counteracts boundary layer temperature advection and opposes the cyclogenesis. In his no-flux experiment with the latter, cyclogenesis was stronger than in the experiment with fluxes. The second pattern of heating is characterized by upward flux to the northeast or east of the surface low and stable stratification to the west of it. It results in boundary layer stratification changes, larger downward momentum flux that is proportional to frictional boundary layer convergence; that in turn, increases the vertical circulation and the intensity of cyclone. So, in this pattern fluxes intensify cyclogenesis.

In the experiments over the EM, SST and heat fluxes distributions are similar to the second pattern. In the case of 5 Jan, 1987 at 18 h (inception time for the secondary development) cyclone pronounced maxima are noticed to the northeast of the low for both sensible (64 W/m^2) and latent (170 W/m^2) heat fluxes, Figures 12a,b. The cyclone moves from west to east over the sea and the Mediterranean SST increases in this direction (Figure 13). Also, temperature gradients exist between Cyprus and sea (in the

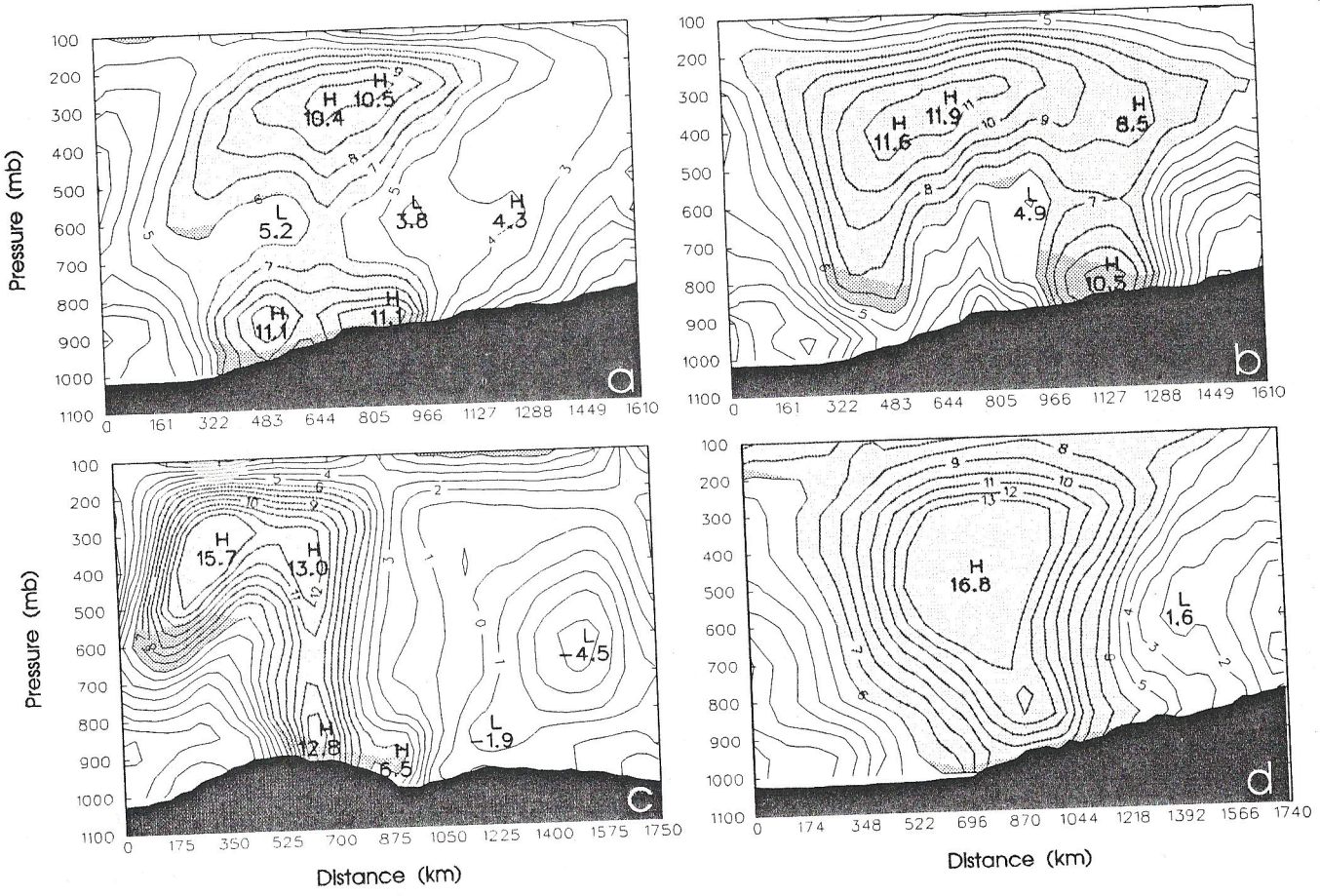

FIGURES 11a,b,c,d As in Figures 10, but for the primary cyclone.

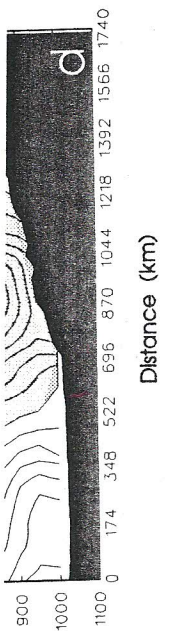

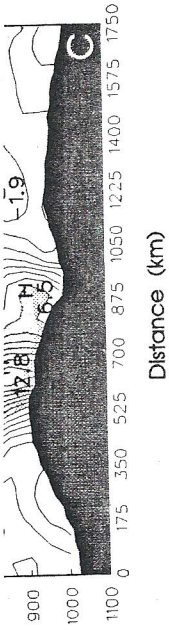

FIGURES 11a, b, c, d As in Figures 10, but for the primary cyclone.

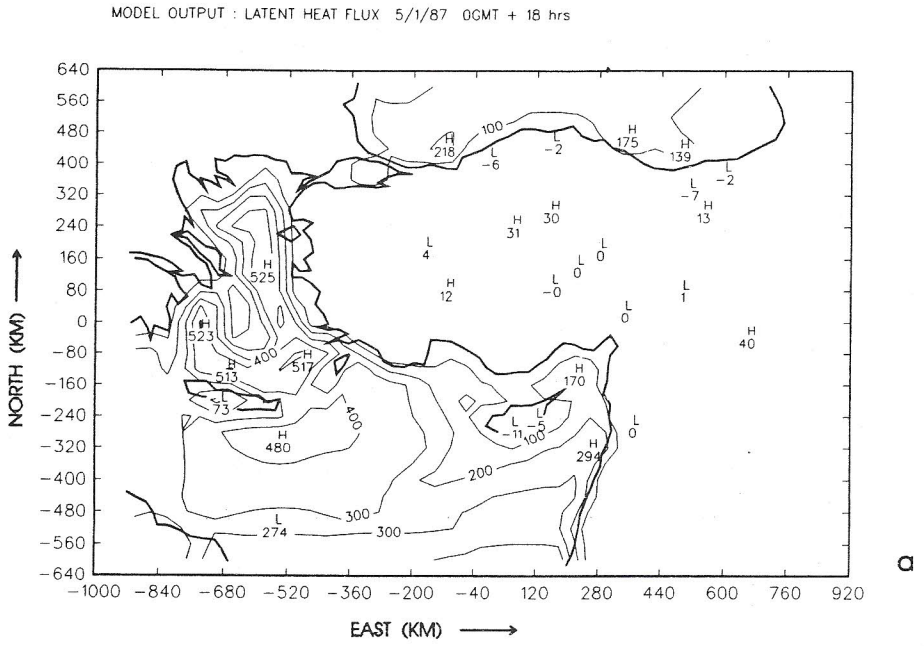

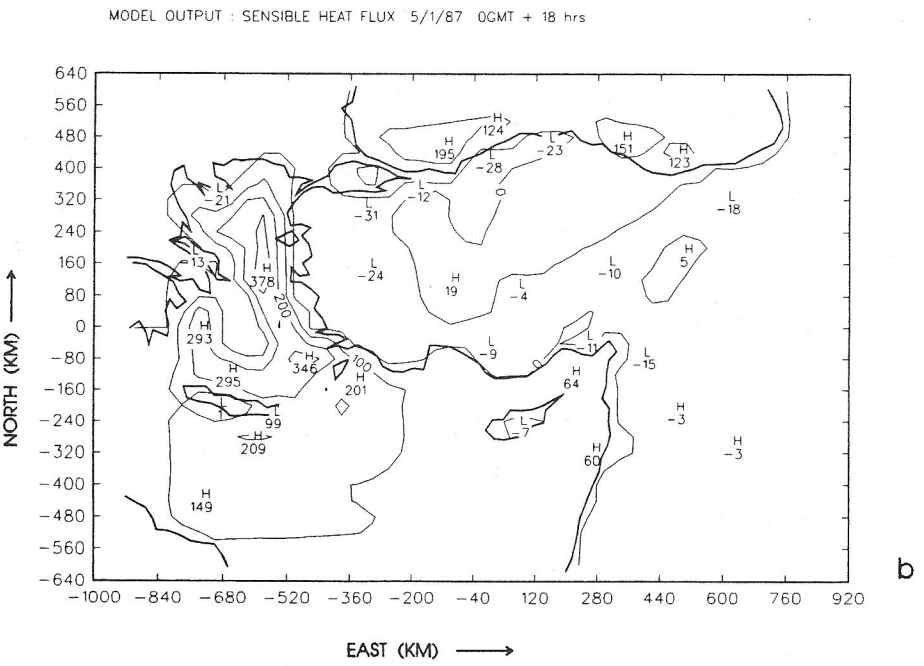

FIGURES 12a, b Distributions of the predicted (a) latent, (b) sensible heat fluxes over the EM for 5 Jan 18 UTC. Contour interval is of 100 Wm^{-2}. Simulation was with 40 km horizontal resolution. Horizontal distances (km) are from central grid point.

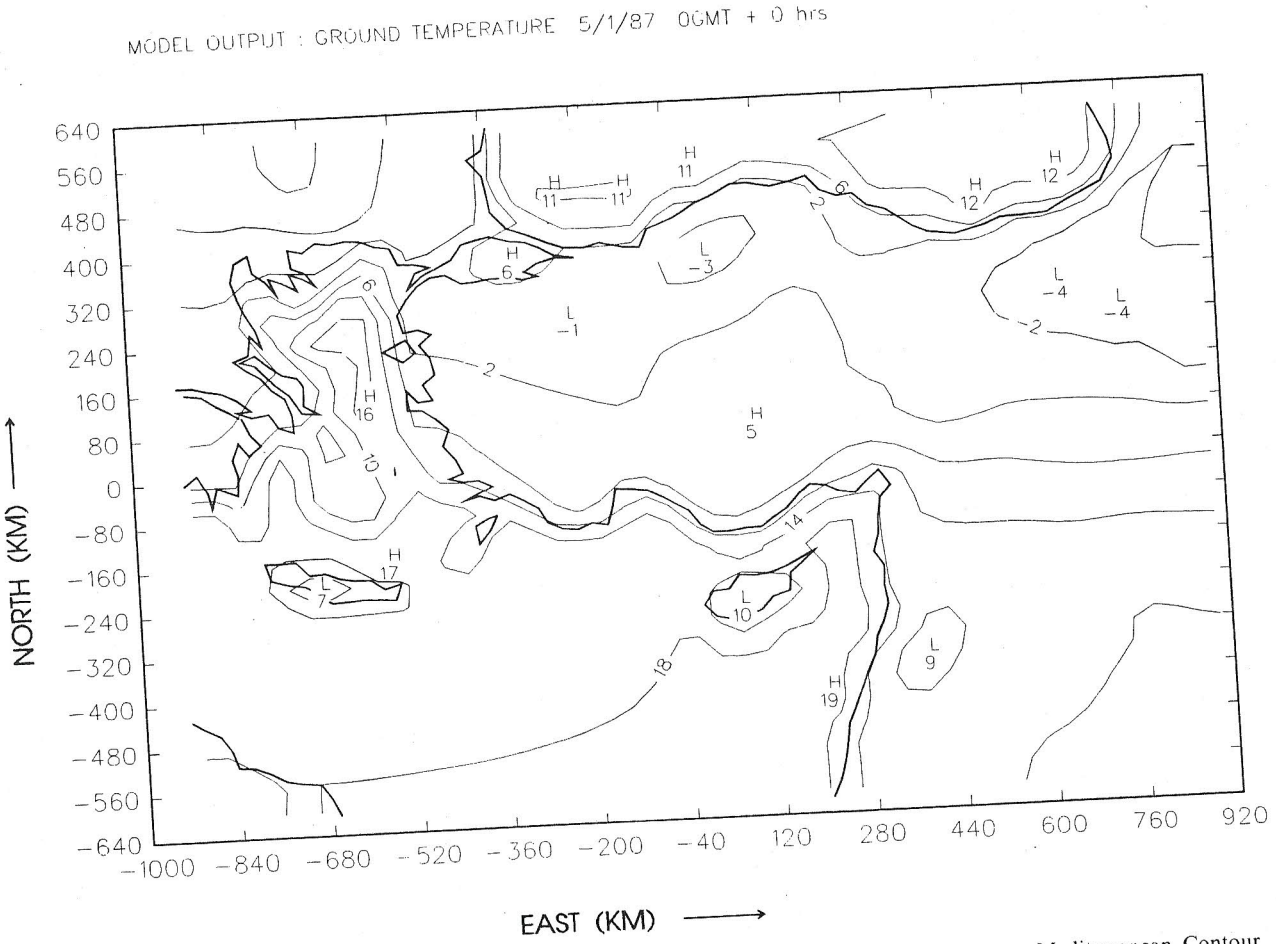

FIGURE 13 Ground and sea surface temperatures for 5 Jan 00 UTC over the model domain at the eastern Mediterranean. Contour interval is 4°C. Horizontal distances as in Figure 12.

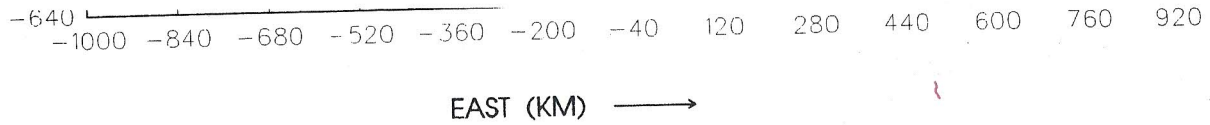

FIGURE 13 Ground and sea surface temperatures for 5 Jan 00 UTC over the model domain at the eastern Mediterranean. Contour interval is 4°C. Horizontal distances as in Figure 12.

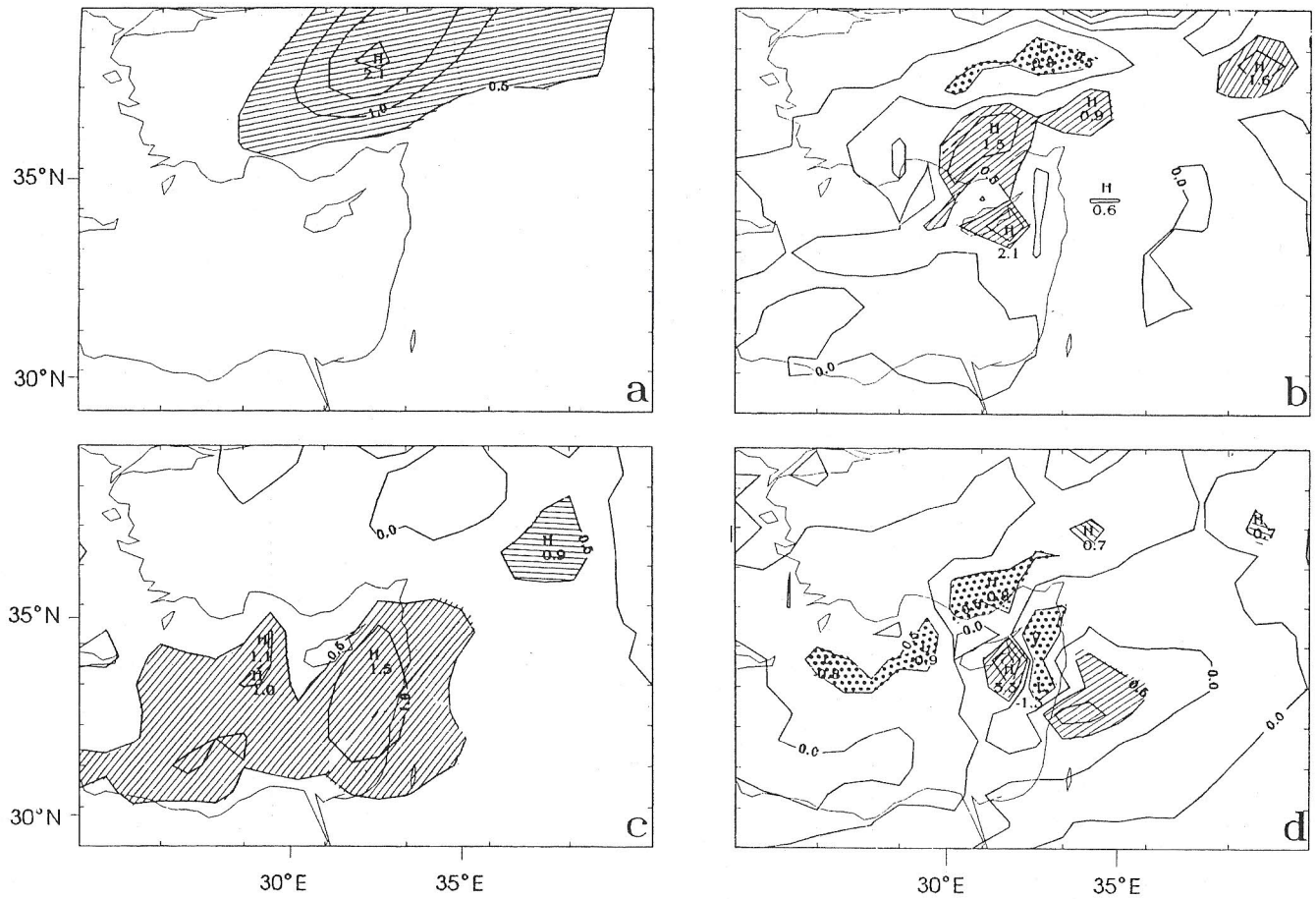

FIGURES 14a, b, c, d Maps of accumulated rainfall contributions by the various factors with the 80 km simulation: (a) 'large scale'; (b) topography only; (c) fluxes only; (d) topography/fluxes interaction. Rainfall is in cms and contour interval is 0.5 cm. Rainfall values below − 0.5 and above + 0.5 cm are shaded by dots and lines respectively.

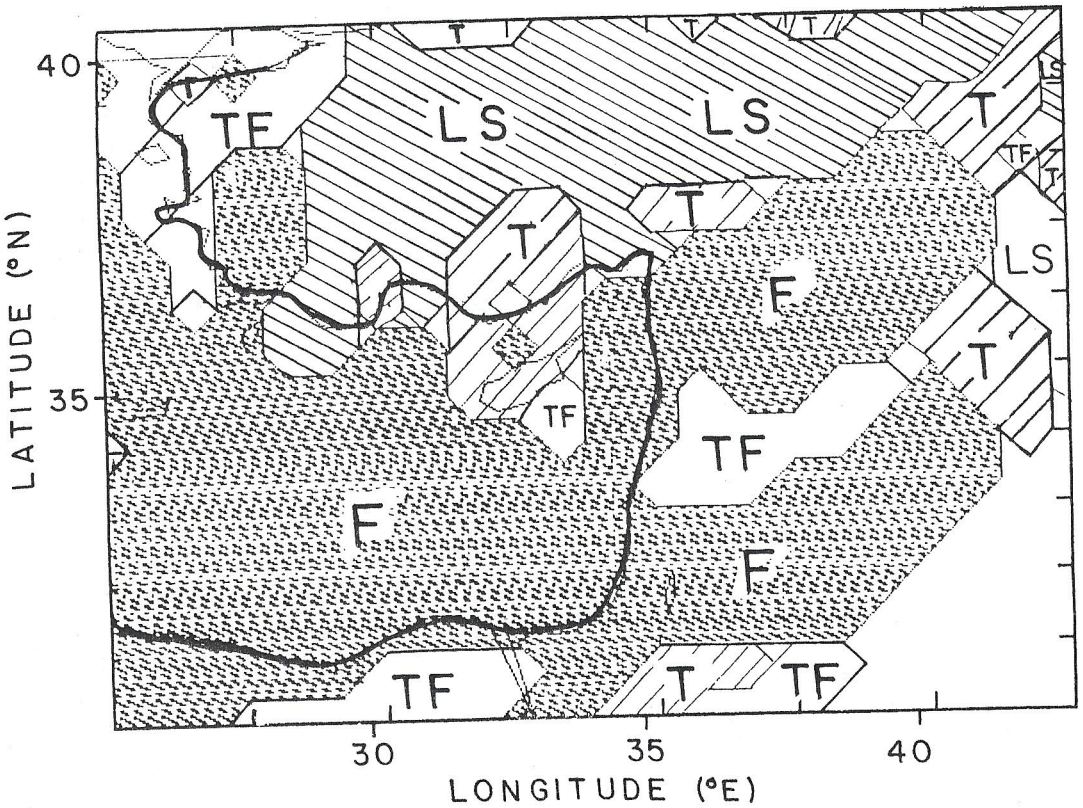

FIGURE 15 Geographical distribution of the dominant contributor for the 36 h simulated rainfall, starting on the 5 Jan 1987 0000 UTC. The 4 contributions are topography (T), surface fluxes (F), fluxes-topography interaction (TF) and the large-scale (LS). Areas unshaded and undenoted were with no rain in the control run.

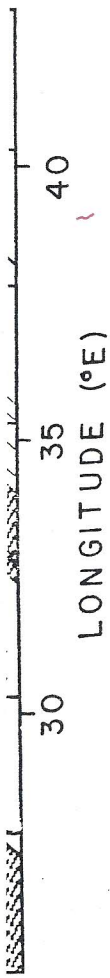

FIGURE 15 Geographical distribution of the dominant contributor for the 36 h simulated rainfall, starting on the 5 Jan 1987 0000 UTC. The 4 contributions are topography (T), surface fluxes (F), fluxes-topography interaction (TF) and the large-scale (LS). Areas unshaded and undenoted were with no rain in the control run.

40 km interval Cyprus is represented by 7–8 points) and the secondary cyclone moves toward warmer water. This pattern corresponds to Nuss's where the idealized cyclone was intensified by fluxes. In addition, the mechanism described by Nuss is in close agreement with the earlier results of the factor separation illustrating that fluxes and fluxes-terrain interactions are the primary factors in the secondary cyclogenesis.

The vorticity cross section through the secondary cyclone for 5 Jan at 24 h shows (not illustrated) that for the 40 km interval the intensity of the low level vorticity associated with local processes is larger than that for the 80 km resolution and also relative to the upper level maximum. In the 80 km experiment the upper level vorticity was stronger. The model with higher resolution better represents local processes and confirms the dominance of the local boundary layer processes for secondary cyclogenesis.

The importance of the sea surface heat fluxes and therefore the secondary development on EM weather is illustrated by the rainfall maps for the first case; the 5 Jan 1987. Figures 14a, b, c, d show the rainfall due to four separated contributions, respectively. Figure 14c, for instance, shows that the major effect of the surface fluxes on precipitation amounts, is to enhance rainfall above the Mediterranean sea, and on the coast to the east. The rainfall maximum adjacent to the coast is probably due to the particular choice of the simulation period, when the cyclone has already approached the EM. The main effect of topography, however, Figure 14b, is the enhancement of rain over the lee of the Turkish mountains and over a very localized area southeast of Cyprus. The island itself is represented in the 80 km model topography by one grid point only; a fact explaining this local maximum. It is not surprising that the topographical contributions include quite large areas of negative rainfall contribution, whereas the fluxes induce mostly positive values.

As indicated by SA who analyzed this case in detail, the joint effect of topography and fluxes (Figure 14d) is strongly expressed in these regions. This synergistic contribution is found to dominate over a significant area of Syria—Israel rather than either of the two factors alone. Figure 14a illustrates the area-restricted rainfall induced by the large-scale only, when excluding the terrain and the fluxes contributions. A summary of the geographical distribution of the dominant factor among the four considered is presented in Figure 15. It shows that the topographic (T) contribution is largest at the lee side of the mountains while the fluxes (F) dominate over sea and downstream. The effect of terrain in unison with sea fluxes is maximized where the synergistic contribution (TF) is indicated. Similar results (not shown) were also found in the other three cases supporting the interpretation to the deepening over the Cyprus region.

6. DISCUSSION AND CONCLUSIONS

Analyzing four cyclonic events in the EM, which were arbitrarily chosen, the following cyclogenetic phenomena were noticed. In all cases, a secondary system appeared, mostly to the south of Cyprus. A series of simulations was used to isolate the effects of surface heat fluxes, topography and their interaction on the two systems using the recently developed factor separation method. The main contributors to the primary cyclone are found to be terrain and terrain-fluxes interaction; for the secondary system over the sea, the fluxes have the strongest effect.

The following picture for the local mechanisms influencing cyclogenesis in the EM, emerges. Two distinct surface developments take part in the cyclogenesis, the northern (primary) cyclone and the southern (secondary) system. Each of the two systems has its own life cycle and dynamics. The primary cyclone tends to move along the southern lee-side of the Turkish mountains with terrain being the main factor influencing its development, possibly through the lee-low mechanism. The Turkish mountains delay and deepen the cyclone or the surface trough associated with it, leading to a quasi-steady state at the lee of the Turkish mountains. After a delay of a few hours most cyclones move eastward while filling.

The generation of the secondary minimum to the south of Cyprus is mainly due to the effect of surface fluxes above the warm Mediterranean sea. In all cases the cyclone was initiated in the same area; a fact which cannot be attributed to the fluxes alone, because they cover a much larger region. It is therefore suggested that the cyclogenetic area of the secondary development was determined by both the fluxes and the mutual interaction contribution of fluxes and topography. In addition, the particular SST pattern with a warm tongue between Cyprus and the EM coast is highly favorable for the intensification as illustrated in the idealized simulations by Nuss (1989).

This study is the first modelling sensitivity attempt to investigate the role of topography and sea fluxes in EM cyclogenesis. It was shown that both the Turkish mountains and the Mediterranean sea fluxes affect the mesoscale structure of the Cyprus low in the following manner. The Turkish mountains delay and deepen the primary cyclone through a lee-low type mechanism, while the Mediterranean fluxes are the dominant factor in generating a secondary deepening south of Cyprus. These results may help us understanding why climate models have difficulties to simulate the strength of the mean trough over the Mediterranean and connected with that to underestimate the precipitation there.

Acknowledgements

We wish to acknowledge NCAR and Dr. Kuo for the help in adopting the PSU/NCAR model at Tel-Aviv University. Thanks to the GIF (German-Israeli Foundation) grant No. I-138-120.8/89 and to the BSF (Binational US-Israel Foundation) grants Nos. 89-00186 and 92-00275 for the supprot to this research. We thank the ECMWF for the analysis data. Helpful comments by the reviewers are acknowledged. Ms. Rachel Duani is thanked for typing the manuscript.

References

Alpert, P. (1984) An early winter subtropical cyclone in the eastern Mediterranean. *Israel J. Earth Sci.*, **33**, 150–156.

Alpert, P. (1989) Baroclinic waveguides and rate of alternation. *J. Atmos. Sci.*, **46**, 3505–3507.

Alpert, P., Neeman, B. U. and Shay-El, Y. (1990a) Climatological analysis of Mediterranean cyclones using ECMWF data. *Tellus*, **42A**, 65–77.

Alpert, P., Neeman, B. U. and Shay-El, Y. (1990b) Intermonthly variability of cyclone tracks in the Mediterranean. *J. Climate*, **3**, 1474–1478.

Alpert, P. and Neeman, B. U. (1992) Cold small scale cyclones in the eastern Mediterranean. *Tellus*, **44A**, 173–179.

Alpert, P., Tsidulko, M. and Stein, U. (1995) Can sensitivity studies yield absolute comparisons for the effects of several processes? *J. Atmos. Sci.*, **52**, 597–601.
Alpert, P. and Warner, T. T. (1986) Cyclogenesis in the eastern Mediterranean. WMO/TMP Report Series No. 22, 95–99.
Anthes, R. A. (1977) A cumulus parameterization scheme utilizing a one-dimensional cloud model. *Mon. Wea. Rev.* **105**, 270–286.
Buzzi, A. and Tibaldi, S. (1978) Cyclogenesis in the lee of the Alps: A case study. *Quart. J. Roy. Meteor. Soc.*, **104**, 271–287.
Egger, J. (1972) Numerical experiments on the cyclogenesis in the Gulf of Genoa. *Beitr. Phys. Atmos.*, **45**, 320–340.
Godev, H. (1970) On the cyclogenetic nature of Earth's orographic form. *Arch. Meteor.Geophys. Bioklim. Ser.A.*, **19**, 299–310.
Keyser, D. and Uccellini, L. W. (1987) Regional models: emerging research tools for synoptic meteorologists. *Bull. Amer. Meteor. Soc.*, **68**, 306–320.
Kuo, H. L. (1974) Further studies of the parameterization of the influence of cumulus convection on large-scale flow. *J. Atmos. Sci.*, **31**, 1232–1240.
Levitch, E. and Tzvetkov, E. (1985) A hydrodynamical model for a single rain situation in the eastern Mediterranean. *Israel J. Earth Sci.*, **34**, 86–90.
Nuss, W. A. (1989) Air-sea interaction influences on the structure and intensification of an idealized marine cyclone. *Mon. Wea. Rev.*, **117**, 351–369.
Petterssen, S. (1956) *Weather Analysis and Forecasting*, Vol. 1, *Motion and Motion Systems.* McGraw Hill, New York.
Radinovic, D. (1965) On forecasting of cyclogenesis in the West Mediterranean and other areas bounded by mountain ranges by baroclinic model. *Arch. Meteor. Geophys. Bioklim.*, **A14**, 279–299.
Radinovic, D. (1987) Mediterranean Cyclones and their Influence on the Weather and Climate. WMO, PSMP Report ser, no. 24, 131 pp.
Rassmussen, E. (1979) The polar low as an extropical CISK disturbance. *Quart. J. R. Meteor. Soc.*, **105**, 531–549.
Reiter, E. R. (1975) *Handbook for forecasters in the Mediterranean:* Weather phenomena of the Mediterranean Basin Environ. Pred. Res. Facility, Naval Postgraduate School, Monterey, California 93940.
Shay-El, Y. and Alpert, P. (1991) A diagnostic study of winter diabatic heating in the Mediterranean in relation with cyclones. *Quart. J. R. Meteor. Soc.*, **117**, 715–747.
Smith, R. B. (1984) A theory of lee cyclogenesis. *J. Atmos. Sci.*, **41**, 1159–1168.
Stein, U. and Alpert, P. (1991) Inclusion of sea moisture flux in the Anthes-Kuo cumulus parameterization. *Beitr. Phys. Atmos.*, **64**, 231–243.
Stein, U. and Alpert, P. (1993) Factor separation in numerical simulations. *J. Atmos. Sci.*, **50**, 2107–2115.
Tafferner, A. and Egger, J. (1990) Test of theories of the lee cyclogenesis: ALPEX cases. *J. Atmos. Sci.*, **47**, 2417–2428.
Tibaldi, S., Buzzi, A. and Malguzzi, P. (1980) Orographically induced cyclogenesis: Analysis of numerical experiments. *Mon. Wea. Rev.*, **108**, 1302–1314.
Tibaldi, S., Buzzi, A. and Speranza, A. (1990) Orographic cyclogenesis. *Extratropical Cyclones–The Eric Palmen Memorial Volume*, C. W. Newton and E. O. Holopainen, Eds. Amer. Meteor. Soc., 107–127.
U. K. Met. Office, (1962) Weather in the Mediterranean. Her Majesty's Stationary Office, London.
Zhang, D. -L., and Anthes, R. A. (1982) A high-resolution model of the planetary boundary layer-sensitivity tests and comparisons with SESAME-79 data. *J. Appl. Meteor.*, **21**, 1594–1609.